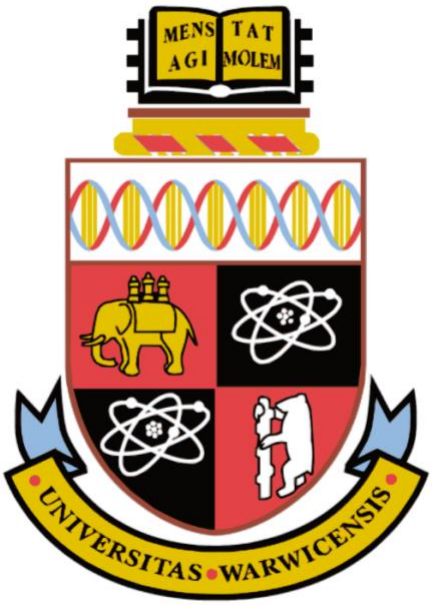

An *In-Silico* Test Rig for Demonstration of Regulatory Compliance in CPAP masks

by

Hossein Shamohammadi

Sina Saffaran

Declan G. Bates

University of Warwick, School of Engineering, Technical Report (Draft 1.0)

17th November 2025

Abstract

Continuous Positive Airway Pressure (CPAP) therapy is a standard treatment for Obstructive Sleep Apnoea (OSA), requiring regulatory verification of adequate CO_2 clearance through bench testing per ISO 17510 standards. This study demonstrates the feasibility of replicating these tests using computational simulation, offering a faster, more cost-effective, and more easily scalable alternative to traditional physical testing. We employed a validated multi-compartmental cardiopulmonary simulator to create digital twins of six healthy subjects and simulated CO_2 rebreathing at baseline and CPAP pressures of 3, 4, 5, and 10 cmH_2O. The simulator outputs showed excellent agreement with values produced on the ISO 17510 benchmark test rig, with end-tidal CO_2 pressures of 37.90-38.04 mmHg (deviation <5% from the 40 mmHg benchmark). End-tidal CO_2 remained stable across all CPAP pressures, consistent with bench test conditions where tidal volume and metabolic rate are held constant. The simulator meets ASME V&V 40 credibility requirements for medical device testing applications. These findings support the use of in-silico methods to supplement or partially replace physical bench testing in regulatory submissions, potentially reducing development time and costs while maintaining (and potentially enhancing) rigorous safety standards for CPAP device evaluation.

Table of Contents

1- Background and Objectives 7

1.1 Background 7
1.2 CO_2 rebreathing Bench Test 7
1.3 Aims and Objectives 8

2- Methods and Modelling 9

2.1 Description of the ICSM Cardiopulmonary Simulator 9
2.2 Modelling Spontaneous Breathing 18
2.3 Model Validation from Previous Work 19
2.4 Incorporation of CPAP Mask Model into the Simulator 23
2.4.1 Exhalation Phase 24
2.4.2 Inhalation Phase 24
2.5 Modelling a cohort of healthy subjects on CPAP 25
2.6 Alignment of the simulator with the bench test rig 26

3- Results 28

3.1 CO_2 Dynamics During Simulated CPAP Therapy 28
3.2 End-Tidal CO_2 Fraction Across CPAP Pressures 28
3.3 End-Tidal CO_2 Pressure Across CPAP Pressures 28
3.4 Baseline Characteristics 34
3.5 Response to CPAP Application 34
3.6 Comparison with Bench Test 34

4- Discussion 35

4.1 CO_2 Dynamics in Bench Testing 35
4.2 Model Accuracy and Acceptable Tolerance 35
4.3 Implications for Virtual Device Testing 36
4.4 Clinical Reality: Expected Differences 36
4.5 Clinical Implications 37

5- Reliability and Credibility of the Simulator (ASME V&V 40 Framework) 38

5.1 Verification 38
5.1.1 Code Verification 38
5.1.2 Solution Verification 38
5.2 Validation 38
5.2.1 Comparative Validation 38
5.2.2 Boundary Condition Validation 39
5.3 Applicability 39
5.4 Summary of V&V 40 Compliance 39

6- Conclusions and Future Work 40

6.1 Key Findings 40
6.2 Divergence from Clinical Conditions 40
6.3 Future Work 41

References 42

Figures

Figure 1: Schematic of bench test rig 8

Figure 2: Diagrammatic representation of the ICSM simulator 9

Figure 3: The effect of varying the parameters of Equation (10) on the pressure volume relationship of the model ($PINSP = 0$) and under mechanical ventilation 13

Figure 4: Patient data distributions compared to simulator outputs while on HFNC, median, interquartile ranges, and actual ranges [32] 20

Figure 5: Patient data compared to simulator outputs [19] 21

Figure 6: Bland-Altman plots comparing the simulator outputs with patients' data. The red dashed line represents the mean difference (bias) between the data and simulator outputs. The green dashed lines indicate the upper and lower 95% limits of agreement, capturing the range within which 95% of the differences line 22

Figure 7: Patient data distributions (black) compared with digital twin outputs (green) while on high-flow nasal cannula therapy (before initiation of noninvasive ventilation [NIV]) and 2 hr after initiation of NIV, median, interquartile ranges, and actual ranges for PaO_2 (A), $PaCO_2$ (B), tidal change in pleural pressure (ΔPpl) (C), and tidal volume (Vt) (D) [17]. 23

Figure 8: Breathing flow pattern of subjects 27

Figure 9: End-tidal CO_2 fraction at baseline (CPAP=0 cmH_2O) 29

Figure 10: End-tidal CO_2 pressure at baseline (CPAP=0 cmH_2O) 29

Figure 11: End-tidal CO_2 fraction at CPAP=3 cmH_2O 30

Figure 12: End-tidal CO_2 pressure at CPAP=3 cmH_2O 30

Figure 13: End-tidal CO_2 fraction at CPAP=4 cmH_2O 31

Figure 14: End-tidal CO_2 pressure at CPAP=4 cmH_2O 31

Figure 15: End-tidal CO_2 fraction at CPAP=5 cmH_2O 32

Figure 16: End-tidal CO_2 pressure at CPAP=5 cmH_2O 32

Figure 17: End-tidal CO_2 fraction at CPAP=10 cmH_2O 33

Figure 18: End-tidal CO_2 pressure at CPAP=10 cmH_2O 33

Tables

Table 1: characteristics of six virtual subjects 26

Table 2: End-tidal CO_2 pressure (mmHg) measured at end-expiration for six virtual subjects at baseline and CPAP pressures of 3, 4, 5, and 10 cmH_2O. 34

1- Background and Objectives

1.1 Background

The use of computational modelling and artificial intelligence (AI) is transforming medical device testing by making it faster, safer, and more cost-effective. A key mission of this initiative is to reduce reliance on animal and physical rig testing and accelerate regulatory approvals.

Continuous Positive Airway Pressure (CPAP) therapy is a standard treatment for Obstructive Sleep Apnoea (OSA), delivering pressurised air to maintain airway patency during sleep. Regulatory standards (ISO 17510) require verification that CPAP masks effectively vent exhaled air and minimise CO_2 rebreathing. This verification is traditionally demonstrated through bench testing—a process that is time-consuming, resource-intensive, and not easily scalable (e.g. for personalized devices).

In-silico approaches offer a promising alternative, allowing these assessments to be conducted virtually. Such simulations can provide rapid, ethical, and highly detailed evaluations that can complement or replace physical testing and support regulatory submissions.

The expected outcome of this project is the quantitative estimation of rebreathed CO_2 volume and end-tidal CO_2 concentration under various breathing conditions.

1.2 CO_2 rebreathing Bench Test

A custom rebreathed CO_2 test rig, designed and manufactured by ResMed, was used to quantify the amount of CO_2 re-inhaled during breathing. The experimental setup, shown in Figure 1, consisted of a breathing simulator representing the lungs, a flow generator, airway tubing, a CPAP mask, and integrated sensors for continuous measurement of flow rates and CO_2 concentration. CO_2 measurements were obtained under several conditions: a baseline configuration (no mask, no ventilatory support) and CPAP pressures of 3, 4, 5, and 10 cmH_2O.

The resulting bench data served as the reference dataset for validation of the *in-silico* models, enabling direct comparison of simulated and experimentally measured rebreathing behaviour across all tested CPAP settings.

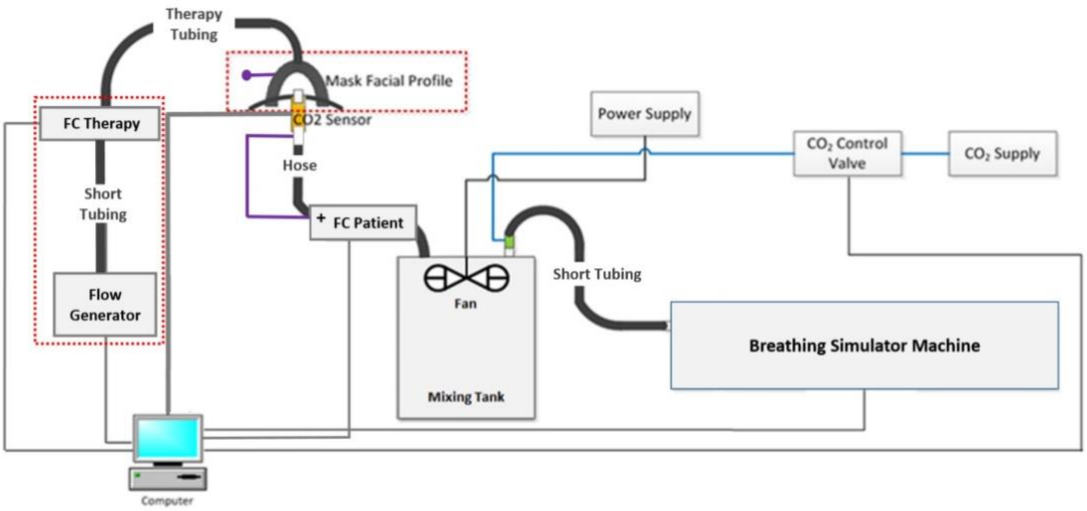

Figure 1:Schematic of bench test rig

1.3 Aims and Objectives

The principal aim of this study is to evaluate whether a high-fidelity computational cardiopulmonary simulator can accurately reproduce the CO_2 rebreathing outcomes obtained from ISO-standardised CPAP bench testing.

Specific objectives are to:

1. Replicate the CO_2 rebreathing bench test using the ICSM simulator
2. Demonstrate compliance with ISO 17510
3. Quantitatively estimate rebreathed CO_2 volume and end-tidal CO_2 concentration under various breathing conditions.

2- Methods and Modelling

2.1 Description of the ICSM Cardiopulmonary Simulator

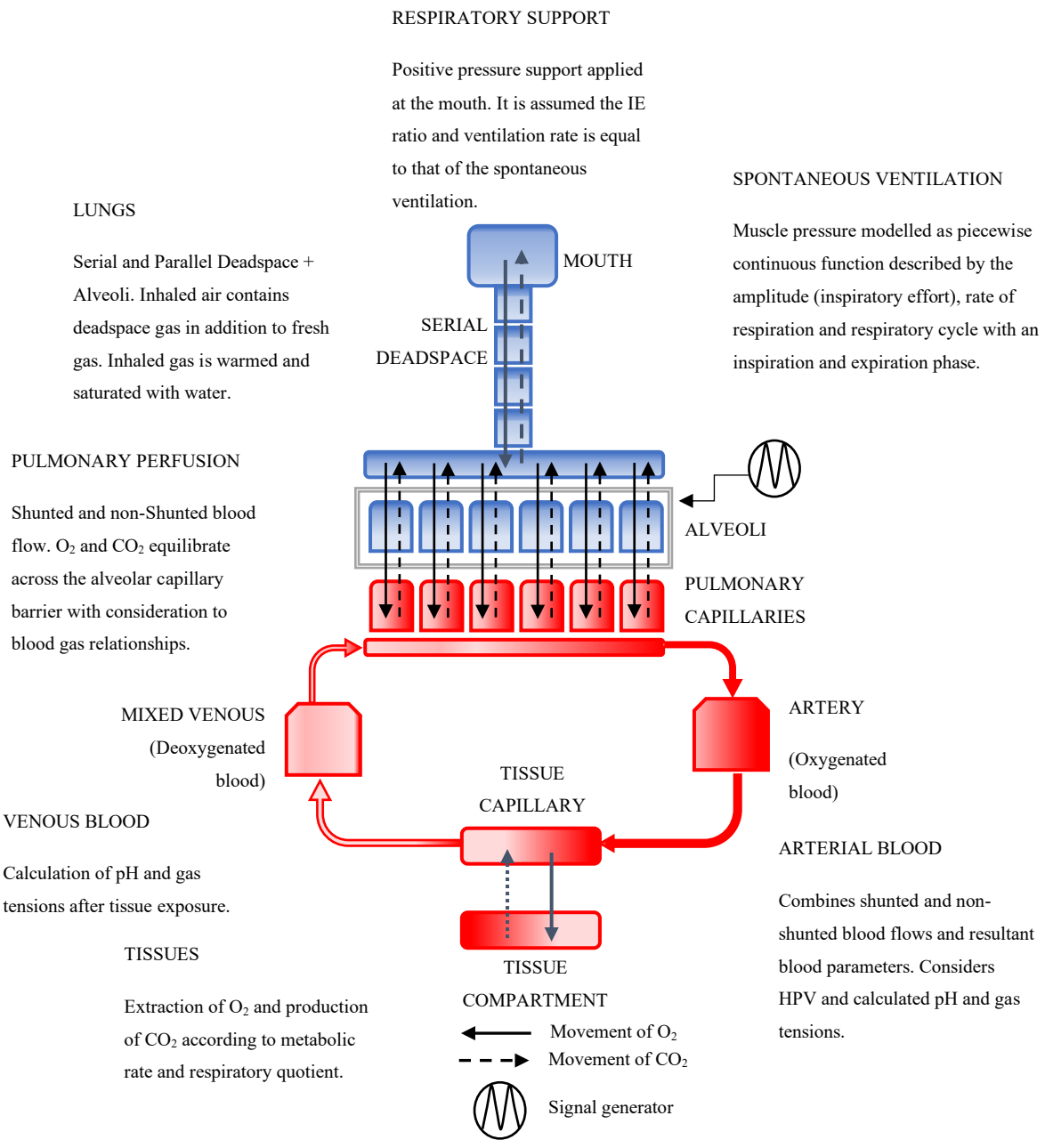

Figure 2: Diagrammatic representation of the ICSM simulator

The simulator employed in this paper has been in continuous development over the past 25 years and has been applied and validated in a number of different studies [1]–[13]. It has previously been employed to simulate patients with COVID-19 [14], chronic obstructive pulmonary disease (COPD) [15], acute respiratory distress syndrome (ARDS) [8], [16], and acute hypoxemic respiratory failure (AHRF) [17]–[19]. The model is organised as a system of several components (see Figure 2: Diagrammatic representation of the ICSM simulator), each component representing different aspects of pulmonary dynamics and blood gas transport, e.g. the transport of air in the mouth, the tidal flow in the airways, the gas exchange in the alveolar compartments and their corresponding capillary compartment, the flow of blood in the arteries, the veins, the cardiovascular system, and the gas exchange process in the peripheral tissue compartments. Each component is described as several mass conserving functions and solved as algebraic equations, obtained or approximated from the published literature, experimental data and clinical observations. These equations are solved in series in an iterative manner, so that solving one equation at the current time instant ($\mathrm{t_k}$) determines the values of the independent variables in the next equation. At the end of the iteration, the results of the solution of the final equations determine the independent variables of the first equation for the next iteration.

The iterative process continues for a predetermined time, *T*, representing the total simulation time, with each iteration representing a 'time slice' *t* of real physiological time (set to 10 ms). At the first iteration ($\mathrm{t_k}, \mathrm{k} = 0$), an initial set of independent variables are chosen based on values selected by the user. The user can alter these initial variables to investigate the response of the model or to simulate different pathophysiological conditions. Subsequent iterations ($\mathrm{t_k} = \mathrm{t_{k-1}} + t$) update the model parameters based on the equations below.

The pulmonary model consists of the ventilation equipment, anatomical and alveolar dead space, anatomical and alveolar shunts, ventilated alveolar compartments and corresponding perfused capillary compartments. The pressure differential created by the ventilator or inspiratory muscles (i.e. when modelling spontaneous breathing) drives the flow of gas through the system. The series dead space (SD) is located between the mouth and the alveolar compartments and consists of the trachea, bronchi and bronchioles where no gas exchange occurs. Inhaled gases pass through the SD during inspiration and alveolar gases pass through the SD during expiration. In the model, an SD of volume 150 ml is split into 50 stacked layers of equal volumes (N_{SD} = 50).

Any residual alveolar air in the SD at the end of expiration is re-inhaled as inspiration is initiated. This residual air is composed of gases exhaled from both perfused alveolar compartments (normal perfusion) and the parallel dead space (PD) (alveolar compartments with limited perfusion). Therefore, the size of dead space (SD and PD) can have a significant effect on the gas composition of the alveolar compartments.

Depending on the application, the inhaled air is initially assumed to consist of up to five gases: oxygen (O_2), nitrogen (N_2), carbon dioxide (CO_2), water vapour (H_2O) and a 5th gas (α) used to model additives such as helium or other anaesthetic gases. During an iteration of the model, the flow (*f*) of air to or from an alveolar compartment *i* at time $t_k$is determined by the following equation:

$$f_i = \frac{(P_{trachea} - p_i)}{(R_{L\_aw,\,i})} \qquad \text{for } i = 1, \ldots, N_A \tag{1}$$

and

$$f_{SD} = \sum_{i=1}^{N_A} f_i \tag{2}$$

is the total flow, where N_A is the total number of alveolar compartments (for the results in this study, N_A = 100). During inhalation, $f_{SD} > 0$, while during exhalation $f_{SD} < 0$.

In the above equations:

$R_{L\_aw,\,i}$ is the lower airway resistance, and is equal to $R_B + R_{A,i}$ where R_B is the resistance of the bronchi and bronchioles, and $R_{A,i}$ is the inlet resistance of the i^{th} alveolar compartment which is defined by:

$$R_{A,i} = m_i R_{A0} \tag{3}$$

where R_{A0} corresponds to the default bronchial inlet resistance of an alveolar compartment. R_{A0} is normally distributed around the mean value of $10^{-7} \times N_A$ (the inlet resistance is higher for a model with more compartments as the volume of each compartment decreases) for a healthy lung. m_i is a coefficient of the airway resistance, representing a dynamic change in airway resistance and is determined by the equation:

$$m_i = \begin{cases} 1, & t_{o,i} \le 0 \\ 10^{15}, & t_{o,i} > 0 \end{cases} \qquad \text{for } i = 1, \ldots, N_A \tag{4}$$

where

$$\mathrm{t_{o,}}_i = \begin{cases} \mathrm{t_{o,}}_i - t\,, & P_{trachea} \geq \mathrm{TOP}_i \\ \tau_{c,i}, & P_{trachea} < \mathrm{TOP}_i \end{cases} \quad \text{for} i = 1, \ldots, N_A \tag{5}$$

$P_{trachea}$ is the pressure at the trachea which is calculated as:

$$P_{trachea} = \begin{cases} P_{inlet} - \left(\frac{P_{inlet} - P_{lungs}}{R_{aw}} \times R_{U\_aw}\right) & Inhalation \\ P_{inlet} - \left(\frac{P_{lungs} - P_{inlet}}{R_{aw}} \times R_{L\_aw}\right) & Exhalation \end{cases} \tag{6}$$

where $P_{inlet} = P_{atm}$ (in the absence of external support) (7)

$$P_{lungs} = \sum_{i=1}^{N_A} \left(\frac{p_i}{\mathrm{R_{L\_aw,}}\, i}\right) \times R_{L\_aw} \tag{8}$$

$$R_{L\_aw} = \frac{1}{\sum_{i=1}^{N_A} \left(\frac{1}{\mathrm{R_{L\_aw,}}\, i}\right)} \tag{9}$$

R_{U_aw} is the upper airway resistance which represents the nasal cavity, oral cavity and trachea and R_{aw} is the total respiratory airway resistance (i.e. R_{U_aw} + R_{L_aw}).

Lung pressure (P_{lungs}) results from the summation of the flow at each alveolar compartment multiplied by the equivalent resistance of the lower airways (R_{L_aw}), i.e., from the end of the trachea to the lungs.

p_i is the pressure in the i^{th} alveolar compartment. Each alveolar compartment has a unique and configurable alveolar stiffness (S_i), alveolar inlet resistance, vascular resistance, extrinsic (interstitial) pressure (P_{ext}), threshold opening pressure and threshold closing pressure. For the i^{th} compartment of N alveolar compartments, the pressure p_i is determined by equation (10) at a given volume of v_i in millilitres:

$$p_i(\mathrm{t_k}) = P_{atm} + S_i(v_i(\mathrm{t_k}) - V_c)^2 - P_{ext,i} + P_{INSP}(\mathrm{t_k}) \quad \text{for } i = 1, \ldots, N_A \tag{10}$$

where

$$S_i = k_i {N_A}^2/200000 \quad \text{and} \quad V_c = 0.2V_{FRC}/N_A \tag{11}$$

The alveolar compartments are arranged in parallel and interact with the series of dead space with respect to the movement of gases. The use of the square of the difference between v_i and V_c causes alveolar pressure to increase at volumes below V_c, leading to exhalation and a tendency to "snap shut" (the pressure with respect to volume is thus a U-shaped curve) [20].

P_{ext} (per alveolar unit, in cmH2O) represents the effective net pressure generated by the sum of the effects of factors outside each alveolus that act to distend that alveolus; positive components include the outward pull of the chest wall, and negative effects include the compressive effect of interstitial fluid within the pleural cavity. Incorporating P_{ext} in the model allows us to replicate the situation of alveolar units that have less structural support or that have interstitial oedema and thus have a greater tendency to collapse or consolidate. A negative value of P_{ext} indicates a scenario where there is compression from outside the alveolus causing collapse. The parameter S_i is a scalar that determines the intra-alveolar pressure for a given volume (with respect to a constant collapsing volume V_c) and is dependent on the parameter k. The units of S_i are cmH2O ml^{-2}. P_{INSP}, which represents the pressure generated by the respiratory muscles acting on the lung, is described in the next section. Finally, V_c is defined as a "constant collapsing volume" at which the alveolus tends to empty (through Laplace effects) and represents a fundamental mechanical property of tissue and surfactant [20]. V_{FRC} is the end expiratory volume of the lungs.

The effect of the three parameters on the volume–pressure relationship of the alveolar compartments can be observed in Figure 3.

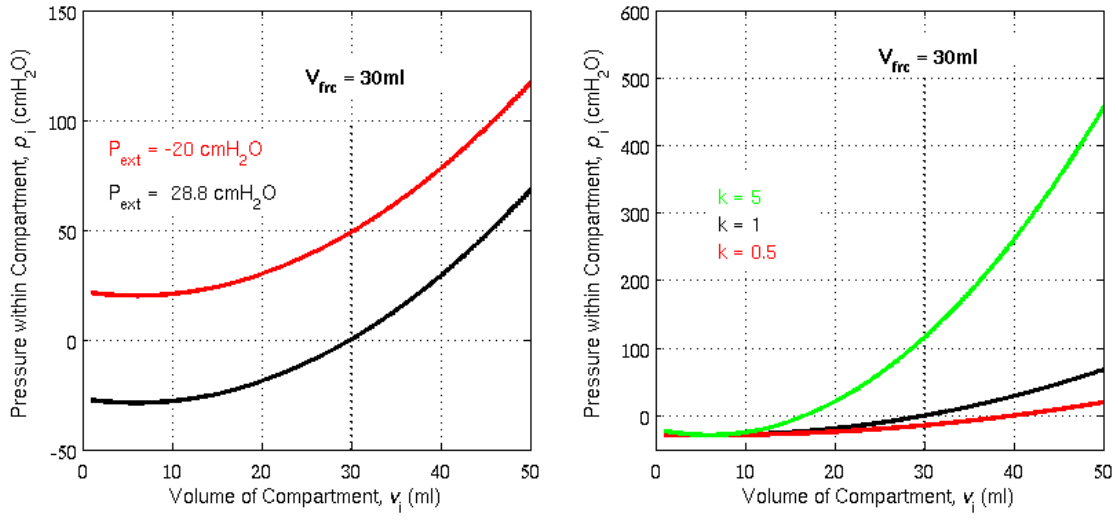

Figure 3: The effect of varying the parameters of Equation (10) on the pressure volume relationship of the model (P_{INSP} = 0) and under mechanical ventilation

The nominal values for ($P_{ext,i}$, S_i) have been determined such that at the end of expiration, the alveolar pressure within the compartment is also equal to zero, i.e. at a pre-set value of functional residual capacity.

We consider each of the parameters mentioned above ($P_{ext,i}$, S_i) to be different yet essential components for representing a diseased lung that affect the volume pressure relationship of the alveolar compartments. For example, for a given volume v_i, increasing S_i increases the corresponding alveolar pressure of the alveolar compartment. When compared to another compartment with a lower S_i, a larger pressure gradient would be needed to drive air into the compartment; thus, effectively the compartment will be behaving as a stiffer lung unit.

Decreasing $P_{ext,i}$ to a negative value increases the alveolar pressure such that the pressure gradient (especially during exhaling) forces the air out of the alveolar compartment until the volume of the compartment collapses (v_i = 0 ml). Note that, in effect, the parameters are influencing the resting volume of the compartments (when the alveolar pressure, p_i, is equal to zero).

TOP_i is a value between 5 and 50 cmH_2O for the i^{th} alveolar compartment. A threshold opening pressure (TOP) at low lung volumes needs to be attained for a collapsed alveolar unit to open. Recruitment is a time dependent process, with different airways recruiting at different times, once the threshold opening pressure has been achieved [21], [22]. The equations within the model are solved iteratively as a discretised system. Each iteration represents a physiological time slice of *t* (10 ms). The time-dependent recruitment phenomenon is achieved in the model by the introduction of a parameter t_o. For collapsed compartments, t_o is set to τ_c which represents the time it would take for collapsed alveoli to open after a threshold pressure is reached. Once $P_{trachea} \geq TOP_i$ is satisfied, the counter t_o decrements during every iteration and triggers the opening of the airway (m_i= 1) as $t_o \leq 0$. Otherwise m_i is set to a high value (10^{15}) to represent a collapsed airway.

N_A (the number of alveolar compartments) is fixed and set by the user (i.e. they do not change during a simulation). Therefore, during a simulation, m_i, chiefly represents the relatively small changes in inlet resistance during tidal ventilation. Furthermore, R_B is also preset and fixed, and does not change during the simulation. The only change in airway resistance which is dynamic is m_i which is dependent on the volume v_i at time(t_k).

Finally, the pulmonary vascular resistance PVR is determined by:

$$\frac{1}{PVR} = \frac{1}{R_{V,1}} + \frac{1}{R_{V,2}} + \cdots + \frac{1}{R_{V,N_A}}, \text{ for } i = 1, \ldots, N_A \quad (12)$$

where the resistance for each compartment $R_{V,i}$ is defined as

$$R_{V,i} = \delta_{Vi} R_{V0} \tag{13}$$

R_{V0} is the default vascular resistance for the compartment with a value of $160 \cdot N_A$ dynes s cm^{-5} min^{-1}, and δ_{Vi} is the vascular resistance coefficient, used to implement the effect of hypoxic pulmonary vasoconstriction.

During gas movement in the SD, the fractions of gases in the layer l of the SD, $F_{l,}$ ($l = 1, \dots, N_{SD}$) are updated based on the composition of the total flow, f_{SD}, and the current composition of $F_{l,}$. If $f_{SD} \geq 0$, then air starts filling from the top layer ($l = 1$) to the bottom layer ($l = N_{SD}$); and vice versa for f_{SD}<0. The volume of gas x, in the i^{th} alveolar compartment ($v_{i,\,x}$), is given by:

$$v_{i,x}(t_k) = \begin{cases} v_{i,x}(t_{k-1}) - f_i(t_k) \cdot \frac{v_{i,x}(t_{k-1})}{v_i(t_k)} & Exhaling \\ v_{i,x}(t_{k-1}) + f_i(t_k) \cdot F_{N_{SD}}(t_k) & Inhaling \end{cases} \quad \text{for } i = 1, \dots, N_A \tag{14}$$

In (14), x is any of the five gases (O_2, N_2, CO_2, H_2O or α). The total volume of the i^{th} alveolar compartment, v_i is the sum of the volume of the five gases in the compartment.

$$v_i(t_k) = v_{i,O2}(t_k) + v_{i,N2}(t_k) + v_{i,CO2}(t_k) + v_{i,H2O}(t_k) + v_{i,\alpha}(t_k) \tag{15}$$

For the alveolar compartments, the tension at the centre of the alveolus and at the alveolar capillary border is assumed to be equal. The respiratory system has an intrinsic response to low oxygen levels in blood which is to restrict the blood flow in the pulmonary blood vessels, known as hypoxic pulmonary vasoconstriction (HPV). This is modelled as a mathematical function, resembling the stimulus response curve suggested by Marshall [23], and is incorporated into the simulator to gradually constrict the blood vessels as a response to low alveolar oxygen tension. The atmospheric pressure is fixed at 101.3 KPa and the body temperature is fixed at 37.2°C.

At each t_k, equilibration between an alveolar compartment and the corresponding capillary compartment is achieved iteratively by moving small volumes of each gas between the compartments until the partial pressures of these gases differ by <1% across the alveolar-capillary boundary. The process includes the nonlinear movement of O_2 and CO_2 across the alveolar capillary membrane during equilibration.

In blood, the total O_2 content (C_{O2}) is carried in two forms, as a solution and as oxyhaemoglobin (saturated haemoglobin):

$$C_{O2}(t_k) = S_{O2}(t_{k-1}) \cdot Huf \cdot Hb + P_{O2}(t_{k-1}) \cdot O_{2sol} \quad (16)$$

In this equation, S_{O2} is the haemoglobin saturation, *Huf* is the Hufner constant, Hb is the haemoglobin concentration and O_{2sol} is the O_2 solubility constant. The following pressure-saturation relation, as suggested by [24] to describe the O_2 dissociation curve, is used in this model:

$$SaO_2(t_k) = \left(((PaO_2^3(t_{k-1}) + 150 \cdot PaO_2(t_{k-1}))^{-1} \times 23400) + 1\right)^{-1} \quad (17)$$

SaO_2 is the saturation of the haemoglobin in blood and $PaO_2$is the partial pressure of oxygen in the blood. As suggested by [25], PaO_2 has been determined with appropriate correction factors in base excess BE, temperature T and pH (7.5005168 = pressure conversion factor from KPa to mmHg):

$$PaO_2(t_k) = 7.5006168 \cdot PaO_2(t_{k-1}) \cdot 10^{[0.48(pH(t_{k-1})-7.4)-0.024(T-37)-0.0013 \cdot BE]} \quad (18)$$

The CO_2 content of the blood (C_{CO2}) is deduced from the plasma CO_2 content ($C_{CO2plasma}$) [26] by the following equation:

$$C_{CO2}(t_k) = C_{CO2plasma}(t_{k-1}) \cdot \left[1 - \frac{0.0289 \cdot Hb}{(3.352 - 0.456 \cdot SaO_2(t_k)) \cdot (8.142 - pH(t_{k-1}))}\right] \quad (19)$$

where SaO_2 is the O_2 saturation, Hb represents the haemoglobin concentration, and pH is the blood pH level. The coefficients were determined as a standardized solution to the McHardy version of Visser's equation [27], by iteratively finding the best fit values to a given set of clinical data. The value of $C_{CO2plasma}$ is deduced using the Henderson-Hasselbach logarithmic equation for plasma C_{CO2} [28]:

$$C_{CO2plasma}(t_k) = 2.226 \cdot s_{CO2} \cdot PaCO_2(t_{k-1}) \left(1 + 10^{(pH(t_{k-1}) - pK')}\right) \quad (20)$$

where s_{CO2} is the plasma CO_2 solubility coefficient and pK' is the apparent pK (acid dissociation constant of the CO_2 bicarbonate relationship). $PaCO_2$ is the partial pressure of CO_2 in plasma and '2.226' refers to the conversion factor from millimoles per litre to ml/100ml. [28] gives the equations for s_{CO2} and pK' as:

$$s_{CO2} = 0.0307 + 0.0057 \cdot (37 - \mathrm{T}) + 0.00002 \cdot (37 - \mathrm{T})^2 \quad (21)$$

$$\mathrm{pK'} = 6.086 + 0.042 \cdot (7.4 - \mathrm{pH}(\mathrm{t_{k-1}})) + (38 - \mathrm{T}) \cdot \left(0.00472 + \left(0.00139 - (7.4 - \mathrm{pH}(\mathrm{t_{k-1}}))\right)\right) \quad (22)$$

$\mathrm{PaCO_2}(\mathrm{t_k})$ is determined by incorporating the standard Henry's law and the s_{CO2} (the CO_2 solubility coefficient above). For pH calculation, the Henderson Hasselbach and the Van Slyke equation [29] are combined. Below is the derivation of the relevant equation. The Henderson-Hasselbach equation (governed by the mass action equation (acid dissociation)) states that:

$$\mathrm{pH} = \mathrm{pK} + \log\left(\frac{bicarbonateconcentration}{carbonicacidconcentration}\right) \quad (23)$$

Substituting pK=6.1 (under normal conditions) and the denominator $(0.225 \cdot \mathrm{PaCO_2})$ (acid concentration being a function of CO_2 solubility constant 0.225 and $PaCO_2$ (in kPa)) gives:

$$\mathrm{pH}(\mathrm{t_k}) = 6.1 + \log\left(\frac{\mathrm{HCO_3}(\mathrm{t_{k-1}})}{0.225 \cdot \mathrm{PaCO_{2(t_k)}}}\right) \quad (24)$$

For a given pH, base excess (BE), and haemoglobin content (Hb), HCO_3 is calculated using the Van-Slyke equation, as given by [29]:

$$\mathrm{HCO_3}(\mathrm{t_k}) = \left((2.3 \times \mathrm{Hb} + 7.7) \times (\mathrm{pH}(\mathrm{t_k}) - 7.4)\right) + \frac{\mathrm{BE}}{(1 - 0.023 \times \mathrm{Hb})} + 24.4 \quad (25)$$

The capillary blood is mixed with arterial blood using the equation below which considers the anatomical shunt (Sh) with the venous blood content of gas x ($C_{v,\,x}$), the non-shunted blood content from the pulmonary capillaries ($C_{cap,\,x}$), arterial blood content ($C_{a,\,x}$), the arterial volume (v_a) and the cardiac output (CO).

$$\mathrm{C_{a,\,x}}(\mathrm{t_k}) = \frac{\mathrm{CO}(\mathrm{t_k}) \cdot \left(Sh \cdot \mathrm{C_{v,\,x}}(\mathrm{t_k}) + (1 - Sh) \cdot \mathrm{C_{cap,\,x}}(\mathrm{t_k})\right) + \mathrm{C_{a,\,x}}(\mathrm{t_k}) \cdot (v_a(\mathrm{t_k}) - \mathrm{CO}(\mathrm{t_k}))}{v_a(\mathrm{t_k})} \quad (26)$$

The peripheral tissue model consists of a single tissue compartment, acting between the peripheral capillary and the active tissue (undergoing respiration to produce energy). The consumed O_2 (V_{O2}) is removed, and the produced CO_2 (V_{CO2}) is added to this tissue compartment. As per the alveolar equilibration, peripheral capillary gas partial pressures reach equilibrium with the tissue compartment partial pressures, with respect to the nonlinear movement of O_2 and CO_2. Metabolic production of acids, other than carbonic acid via CO_2 production, is not modelled. After peripheral tissue equilibration of gases, the venous

calculations of partial pressures, concentrations and pH calculations are done using comparable equations to those above.

A simple equation of renal compensation for acid base disturbance is incorporated. The base excess (BE) of blood under normal conditions is zero. BE increases by 0.1 per time slice if pH falls below 7.36 (to compensate for acidosis) and decreases by 0.1 per time slice if pH rises above 7.4 (alkalosis).

The net effect of these components of the simulation is that the defining, clinical features of acute respiratory disease may be observed in the model: alveolar gas-trapping (with intrinsic PEEP), collapse-reopening of alveoli (with gradual reabsorption of trapped gas if re-opening does not occur), limitation of expiratory flow etc.

Shunt estimates the portion of blood that bypasses the lungs without participating in gas exchange. Shunt equation is:

$$Shunt = \frac{C_cO_2 - C_aO_2}{C_cO_2 - C_vO_2} \tag{27}$$

Where C_cO_2 is Oxygen content in end-capillary blood, C_aO_2 is Oxygen content in arterial blood, and C_vO_2 is Oxygen content in mixed venous blood.

2.2 Modelling Spontaneous Breathing

The pressure at the airway opening (i.e. nares or mouth) is relatively constant at atmospheric pressure, while the alveolar pressure value varies during inspiration and expiration. The active contraction of the respiratory muscles during inspiration generates a negative alveolar pressure relative to the atmospheric pressure. The variable P_{INSP}, which represents the pressure generated by the respiratory muscles acting on the lung, is modelled as a piecewise function as described in [30] and adapted from [31]. The function consists of a parabolic profile during the inspiration phase of the respiratory cycle, representing the progressive increase in pressure exerted by the respiratory muscles, followed by an exponential profile during the expiration phase of the respiratory cycle, characterizing the passive relaxation of the muscles. During a single respiratory cycle, P_{INSP} at time $\mathrm{t_k}$, is calculated as

$$P_{INSP}(\mathrm{t_k}) = \begin{cases} \frac{-P_{min}}{T_I.T_E}.\mathrm{t_k}^2 + \frac{P_{min}.T}{T_I.T_E}.\mathrm{t_k} & \mathrm{t_k} \in \lfloor 0, T_I \rfloor \\ \frac{P_{min}}{1-e^{-\frac{T_E}{\tau}}}.\left(e^{-\frac{(\mathrm{t_k}-T_I)}{\tau}} - e^{-\frac{T_E}{\tau}}\right) & \mathrm{t_k} \in \lfloor T_I, T \rfloor \end{cases} \tag{28}$$

P_{INSP} decreases from zero to its minimum end-inspiratory value (P_{min}) (i.e., maximum effort) during inspiration and returns to zero at the end of expiration. T is calculated from the set respiratory rate, RR, (T = 60/RR). T_I and T_E are the duration of inspiration and expiration, such that ($T = T_I + T_E$). T_I is calculated from ($T_I = T * DC$) where DC is the duty cycle (in the range of 0.25 to 0.5). τ is the time constant of the expiratory profile and is set to Te/RR.

The resulting alveolar pressure p_i depends on P_{INSP}, as well as on the pressures of the gases within the compartment, the stiffness of the compartment (S_i), and parameter P_{ext} which represents extrinsic pressures acting on the compartment.

2.3 Model Validation from Previous Work

The computational simulator employed in this study has been extensively validated across multiple respiratory support modalities and patient populations.

In previous work [9]–[13], we adapted a detailed computational model of the cardiopulmonary system to investigate the effects of invasive and non-invasive respiratory support methods, including High-Flow Nasal Cannula (HFNC) therapy and Non-Invasive Ventilation (NIV) therapies in both healthy and diseased states. The simulator was calibrated against experimental and clinical data, and digital twins were created to replicate patient responses in a variety of conditions, including COVID-19 [14], chronic obstructive pulmonary disease (COPD) [15], acute respiratory distress syndrome (ARDS) [8], [16], and acute respiratory failure (ARF) [17], [19], [32]. The simulator offers several advantages, including the ability to define multiple alveolar compartments with unique mechanical characteristics such as configurable alveolar collapse and stiffening, gas-exchange disruption, pulmonary vasoconstriction, vasodilation, airway obstruction, etc. This allows for the representation of various clinical features of acute lung injury, including ventilation-perfusion mismatch, physiological shunt, dead space, alveolar gas trapping with intrinsic positive end-expiratory pressure (PEEP), and alveolar collapse-reopening, among others [9], [10].

Validation examples include:

HFNC validation: Figure 4 shows model outputs compared to 58 patients receiving HFNC at 60 L/min [33], [34], with mean absolute percentage errors of 0.5% for PaO_2, 0.6% for $PaCO_2$, 2.5% for ΔPpl, and 4.5% for VT [32].

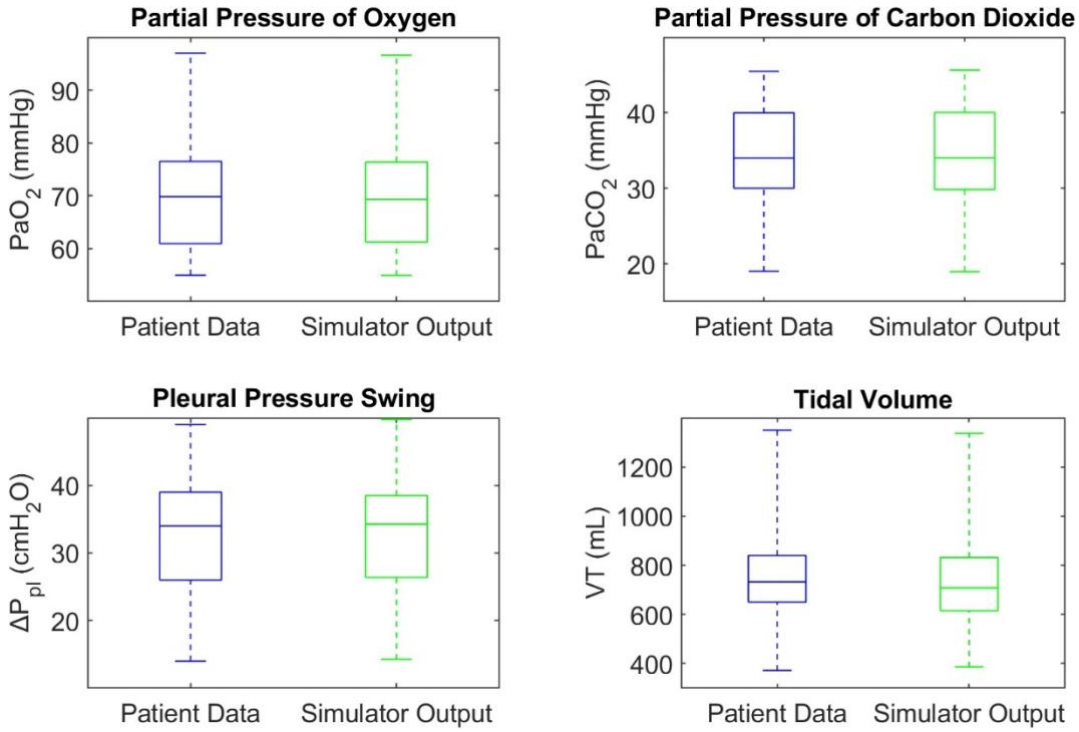

Figure 4: Patient data distributions compared to simulator outputs while on HFNC, median, interquartile ranges, and actual ranges [32]

HFNC validation: Figure 5 presents comparisons of model outputs against clinical measurements [35], [36], yielding mean absolute percentage error / bias values of 1.42% / 1.29 mmHg for PaO_2, 0.91% / 0.35 mmHg for $PaCO_2$, 3.64% / 0.25 cmH_2O for ΔPpl, and 7.76% / 34.45 mL for VT [19].

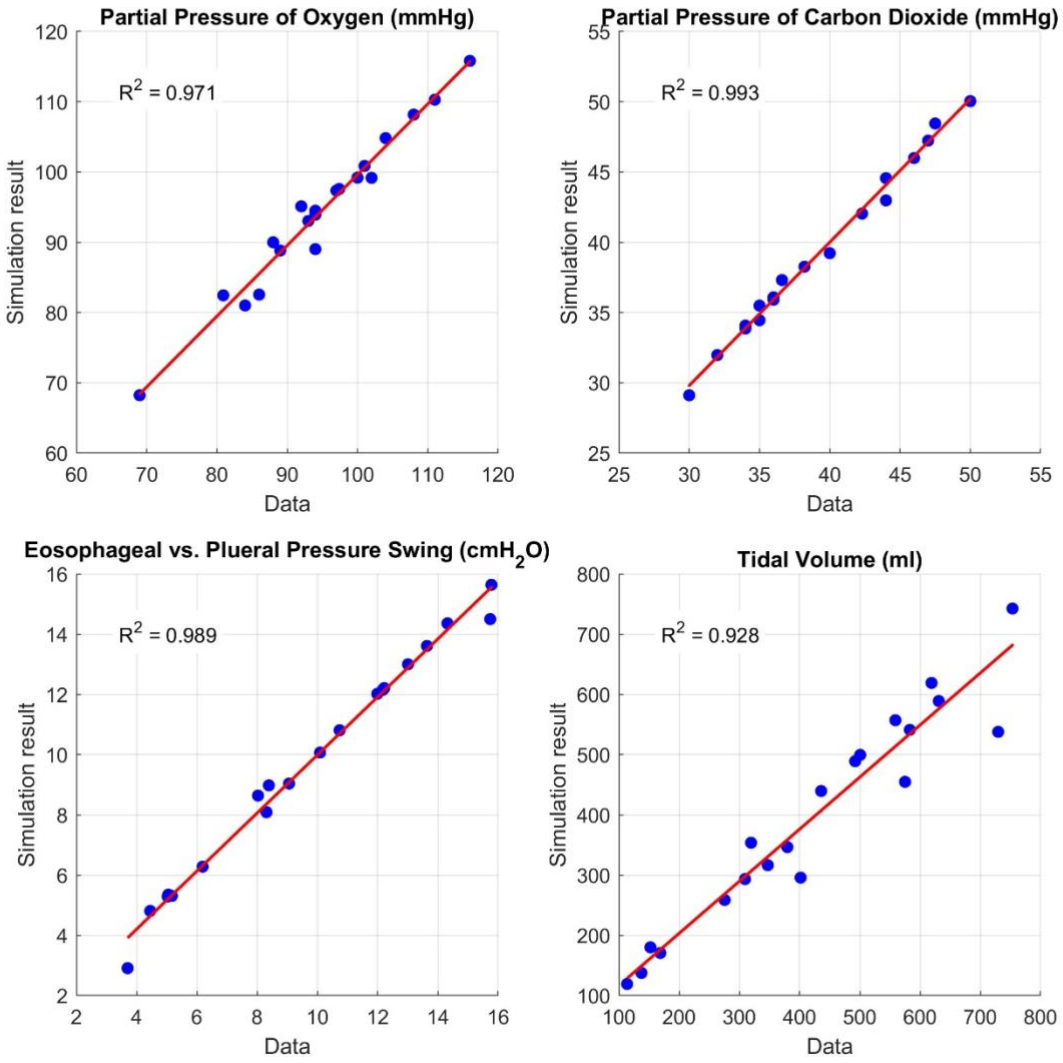

Figure 5: Patient data compared to simulator outputs [19]

Multi-condition HFNC validation: Across 30 patients (AHRF and sepsis) [35]–[37], the simulator reproduced patient data at two different flow rates with mean absolute percentage error /bias of 2.33% / 1.96 mmHg for PaO_2, 1.68% / 0.59 mmHg for $PaCO_2$, 6.62% / 0.4 cmH_2O for ΔPpl, and 10.2% / 47.69 mL for VT (Figure 6).

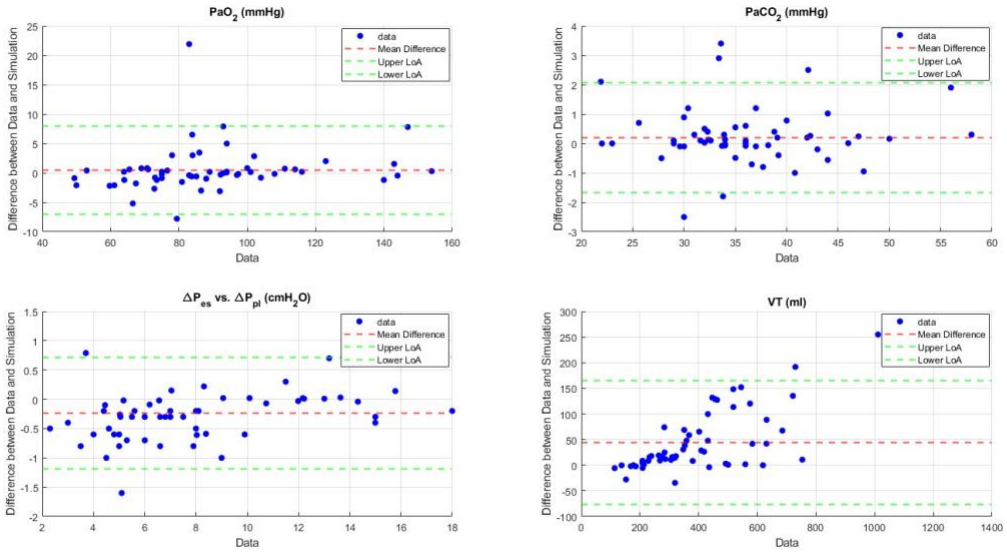

Figure 6:Bland-Altman plots comparing the simulator outputs with patients' data. The red dashed line represents the mean difference (bias) between the data and simulator outputs. The green dashed lines indicate the upper and lower 95% limits of agreement, capturing the range within which 95% of the differences line.

NIV validation: For 2-hour NIV simulations [17], the mean absolute percentage error /bias were 1.21% / 0.36 mmHg (PaO_2), 1.14% / 0.26 mmHg ($PaCO_2$), 1.97% / –0.36 cmH_2O (ΔPpl), and 10.02% / 87.29 mL (VT). The details are in Figure 7.

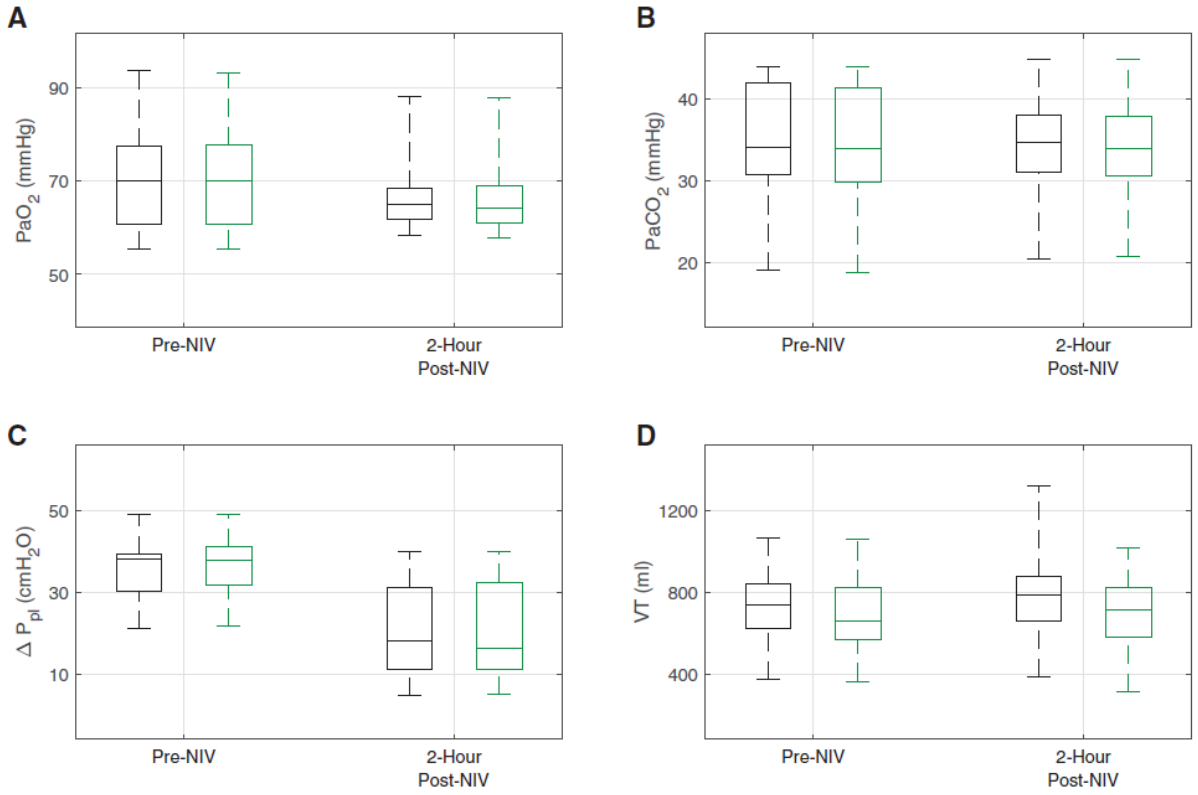

*Figure 7: Patient data distributions (black) compared with digital twin outputs (green) while on high-flow nasal cannula therapy (before initiation of noninvasive ventilation [NIV]) and 2 hr after initiation of NIV, median, interquartile ranges, and actual ranges for PaO_2 (**A**), $PaCO_2$ (**B**), tidal change in pleural pressure (ΔPpl) (**C**), and tidal volume (Vt) (**D**) [17].*

These validation studies collectively demonstrate the simulator's accuracy and its ability to replicate realistic patient responses across a broad range of physiological conditions and respiratory interventions.

2.4 Incorporation of CPAP Mask Model into the Simulator

To replicate the CO_2 rebreathing test conditions, a CPAP mask model was integrated into the computational simulator. The mask compartment represents the volume between the patient's airway opening and the CPAP interface, through which both the supplied fresh flow from the CPAP device and the patient's inspiratory/expiratory flows passes.

The dynamic mass balance for the mask was formulated using instantaneous gas flow rates for each respiratory phase. The total inflow and outflow through the mask satisfy the following relationship:

$$Q_{cpap} = V_{mask} - \left(Q_{patient} + Q_{vent}\right)$$

where V_{mask} is the mask volume, Q_{cpap} the volume of fresh gas delivered by the CPAP device at each time slice, Q_{vent} is the volume of gas venting through intentional leak ports at each time slice, and $Q_{patient}$ is either the inspiratory (Q_{inhale}) or expiratory (Q_{exhale}) volume of gas from the patient, depending on the respiratory phase.

2.4.1 Exhalation Phase

During exhalation, exhaled gas containing CO_2 enters the mask volume. The fractional CO_2 concentration within the mask (F_{maskCO_2}) is updated according to a mass balance between the entering and leaving gas streams:

$$F_{maskCO_2} = \frac{Q_{cpap} \cdot FiCO_2 + Q_{exhale} \cdot FeCO_2 + \left(V_{mask} - \left(Q_{cpap} + Q_{exhale}\right)\right) \cdot F_{maskCO_2}}{V_{mask}}$$

where $FiCO_2$ is the fractional CO_2 concentration in the fresh gas, and $FeCO_2$ is the fractional CO_2 concentration of the exhaled breath.

2.4.2 Inhalation Phase

During inhalation, the patient draws gas from the mask volume, which is continuously replenished by the CPAP device. The corresponding mask CO_2 concentration is:

$$F_{maskCO_2} = \frac{Q_{cpap} \cdot FiCO_2 + (V_{mask} - (Q_{cpap} + Q_{inhale})) \cdot F_{maskCO_2}}{V_{mask}}$$

This set of equations is solved iteratively at each simulation time step, dynamically updating the gas composition within the mask. Identical formulations are applied for F_{maskO_2}, F_{maskN_2} ,and F_{maskH_2O}, ensuring full mass conservation for all gas species.

All mass balance equations are solved synchronously with the core simulator's respiratory mechanics solver, ensuring temporal alignment between pressure–flow dynamics and gas transport within the CPAP mask.

2.5 Modelling a cohort of healthy subjects on CPAP

We adapted this computational simulator to create a virtual cohort of six healthy subjects whose characteristics were representative of the subjects used in a previous experimental study [38]. The virtual cohort consists of an equal number of males and females, with an average age of 33 years, height of 170 cm, and weight of 74 kg, falling within the normal BMI range. Detailed information regarding the cohort is presented in Table 1. Normal lung physiology and respiratory effort are simulated in all cases, with compliance and airway resistance values varying within normal ranges. To derive essential outputs pertaining to respiratory function and gas exchange during normal breathing, the model incorporates equations based on widely accepted physiological principles, enabling the calculation of parameters such as oxygen consumption, cardiac output, vital capacity, functional residual volume, and respiratory system, chest-wall, and lung compliances.

Table 1: characteristics of six virtual subjects

	Subject 1	Subject 2	Subject 3	Subject 4	Subject 5	Subject 6
Sex	M	M	M	F	F	F
Age (year)	22	34	60	33	44	50
Height (cm)	185	178	173	170	164	159
Weight (kg)	75	80	85	76	65	60
BMI	21.9	25.2	28.4	26.5	24.2	23.7
CO (L/min)	5.9	5.6	5.5	5.4	5.2	5.0
VC (ml)	4656	4258	3627	3131	2843	2660
FRC (ml)	3252	3241	3351	2845	2622	2468
R_{aw} ($cmH_2O.s/L$)	3.8	4.3	5	5.8	6.5	7.4
C_{CW} (ml/cmH_2O)	186	170	145	125	114	106
C_L (ml/cmH_2O)	215	178	161	140	126	112
C_{RS} (ml/cmH_2O)	100	87	76	66	60	55
VT (ml)	520	468	463	456	382	345
I:E	1:2	1:2	1:2	1:2	1:2	1:2
RR (bpm)	13	14	15	14	15	16
P/F ratio (mmHg)	474	474	469	472	477	477
PaO_2 (mmHg)	99.5	99.5	98.4	99.2	100.3	100.1
SaO_2 (%)	98	98	98	98	98	98
$PaCO_2$ (mmHg)	36.1	35.7	36.2	35.8	35.7	36.2
pH	7.45	7.45	7.45	7.45	7.45	7.44
Total strain	0.16	0.15	0.14	0.16	0.15	0.14
Stress (ΔP_L) (cmH_2O)	2.4	2.6	2.9	3.3	3.0	3.1
Power (J/min)	0.8	0.9	1.0	1.0	0.9	0.8
ΔP_{pl} (cmH_2O)	5.0	5.3	6.1	6.9	6.4	6.5

CO – Cardiac output | VC – Vital capacity | FRC – Functional residual capacity | R_{aw} – Total airway resistance | C_{CW} – Chest-wall compliance | C_L – Lungs compliance | C_{RS} – Respiratory system compliance | VT – Tidal volume | I:E – Inhalation to Exhalation ratio | RR – Respiratory rate | ΔP_L – Transpulmonary pressure swing | ΔP_{pl} – Pleural pressure swing

2.6 Alignment of the simulator with the bench test rig

To align the simulated subjects with the conditions of the bench test, several physiological and respiratory parameters were adjusted. The inspiratory-to-expiratory (I:E) ratio was modified to 0.54 under baseline conditions and 0.58 during CPAP support to replicate the sinusoidal breathing pattern of the bench test flow generator. The respiratory rate (RR) was fixed at 15 breaths per minute for all simulations. The level of respiratory muscle effort was adjusted to maintain a tidal volume (VT) within the range of 500–510 mL at baseline and across all CPAP pressure levels for each subject in the cohort.

Furthermore, the oxygen consumption (VO_2) was increased from the physiological range of 200–300 $mL \cdot min^{-1}$ to 320 $mL \cdot min^{-1}$ to match the elevated CO_2 production levels used in the

bench test, assuming a constant respiratory quotient (RQ) of 0.8. It is noted that these adjusted values exceed typical resting physiological ranges, particularly for the female subjects. For reference, the normal oxygen consumption in the rest condition in humans is approximately 3.5 $mL \cdot kg^{-1} \cdot min^{-1}$, whereas in the male subjects simulated the average value was 3.9 $mL \cdot kg^{-1} \cdot min^{-1}$ and in the females the average value was 4.8 $mL \cdot kg^{-1} \cdot min^{-1}$.

Additionally, to reproduce the experimental breathing waveform, the simplified sinusoidal flow profile used by the bench test flow generator was implemented in the simulator. This ensured that the simulated breathing waveform closely matched the experimental setup (see Figure 8).

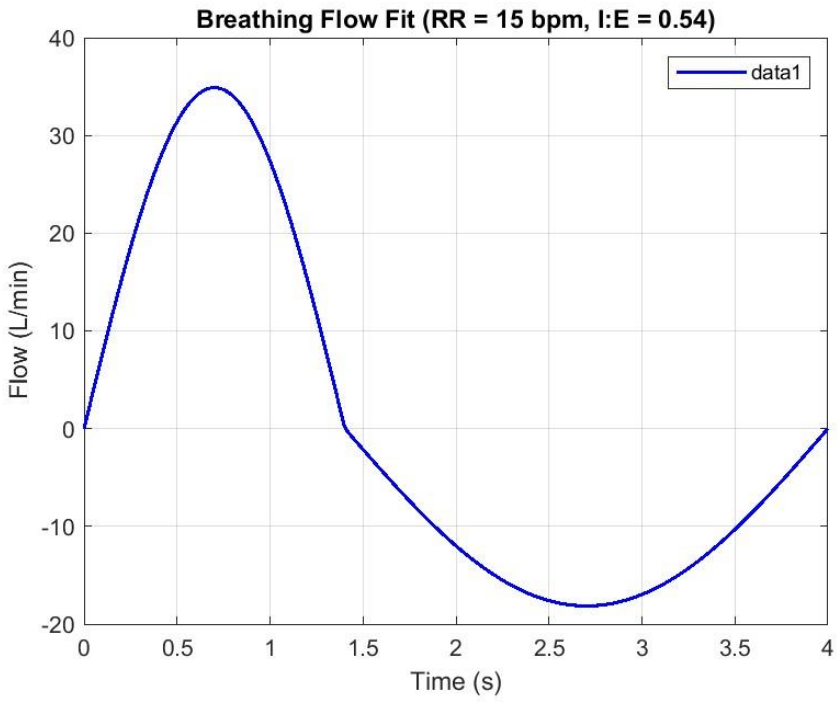

Figure 8: Breathing flow pattern of subjects

3- Results

3.1 CO_2 Dynamics During Simulated CPAP Therapy

The simulator was used to replicate the bench test protocol for CO_2 rebreathing assessment across a virtual cohort of six healthy subjects. Simulations were performed at baseline (no CPAP support) and at four clinically relevant CPAP pressure levels: 3, 4, 5, and 10 cmH_2O. For each condition, both end-tidal CO_2 fraction and end-tidal CO_2 pressure were calculated to assess the mask's ability to prevent CO_2 rebreathing.

3.2 End-Tidal CO_2 Fraction Across CPAP Pressures

Figure 9, Figure 11, Figure 13, Figure 15 , and Figure 17 display the end-tidal CO_2 fraction profiles for the virtual cohort at baseline and at CPAP pressures of 3, 4, 5, and 10 cmH_2O, respectively. These figures illustrate the temporal evolution of CO_2 fraction throughout the respiratory cycle for each subject. Visual inspection of the waveforms demonstrates consistent patterns across subjects, with characteristic rises during expiration and falls during inspiration. The amplitude and shape of the CO_2 fraction curves remained remarkably stable across all CPAP pressure levels, indicating effective venting of exhaled gases throughout the pressure range tested.

3.3 End-Tidal CO_2 Pressure Across CPAP Pressures

Figure 10**,** Figure 12**,** Figure 14**,** Figure 16**,** and Figure 18 present the corresponding end-tidal CO_2 pressure profiles at baseline and CPAP pressures of 3, 4, 5, and 10 cmH_2O, respectively. Similar to the CO_2 fraction data, the pressure waveforms exhibited consistent patterns across subjects and conditions. The end-tidal CO_2 pressure values showed minimal variation across the range of CPAP pressures applied.

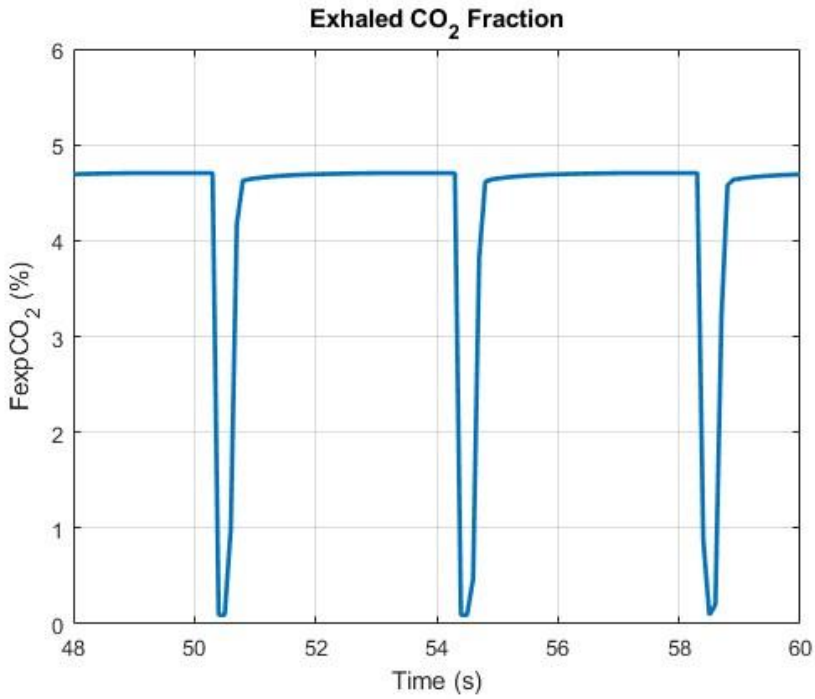

Figure 9: End-tidal CO_2 fraction at baseline (CPAP=0 cmH_2O)

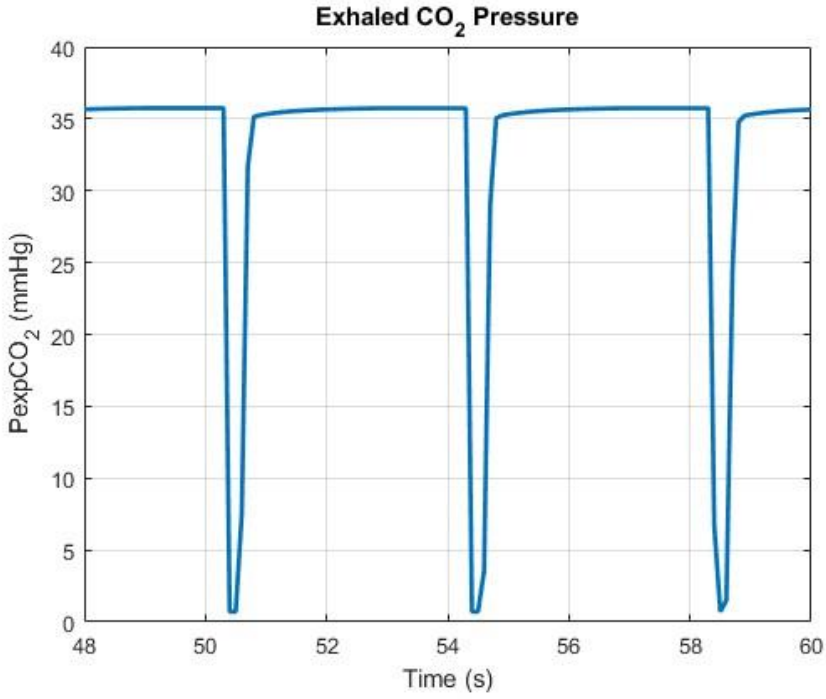

Figure 10: End-tidal CO_2 pressure at baseline (CPAP=0 cmH_2O)

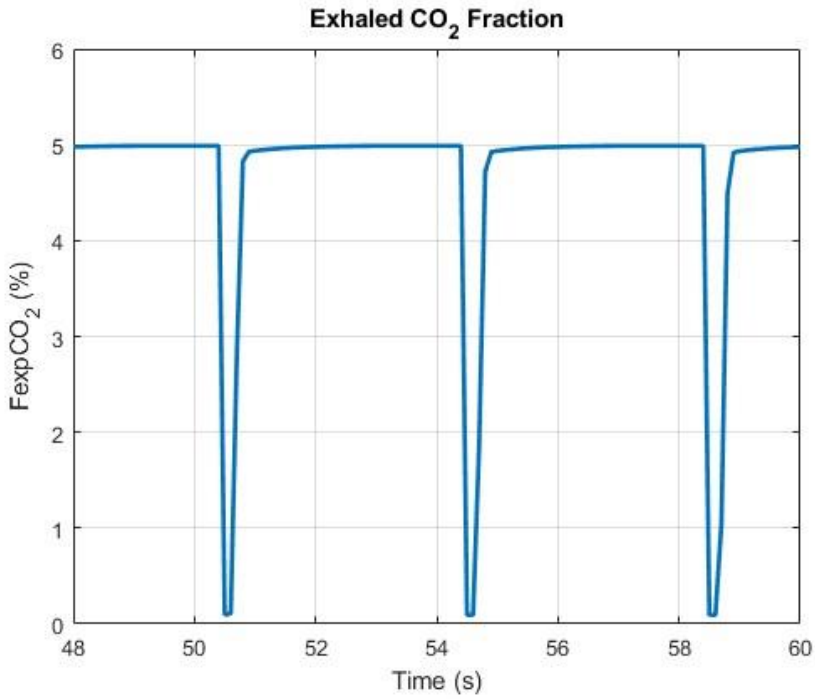

Figure 11: End-tidal CO_2 fraction at CPAP=3 cmH_2O

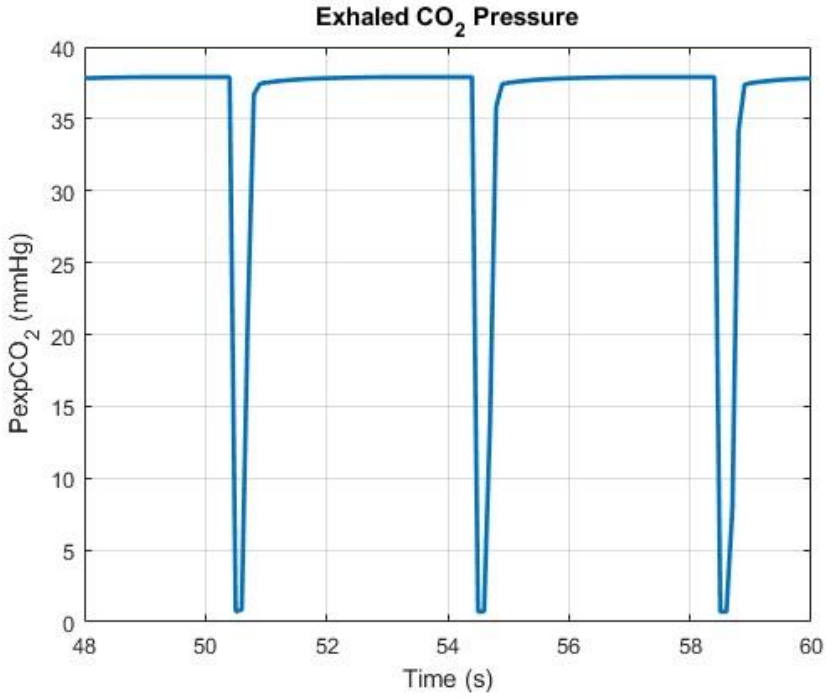

Figure 12: End-tidal CO_2 pressure at CPAP=3 cmH_2O

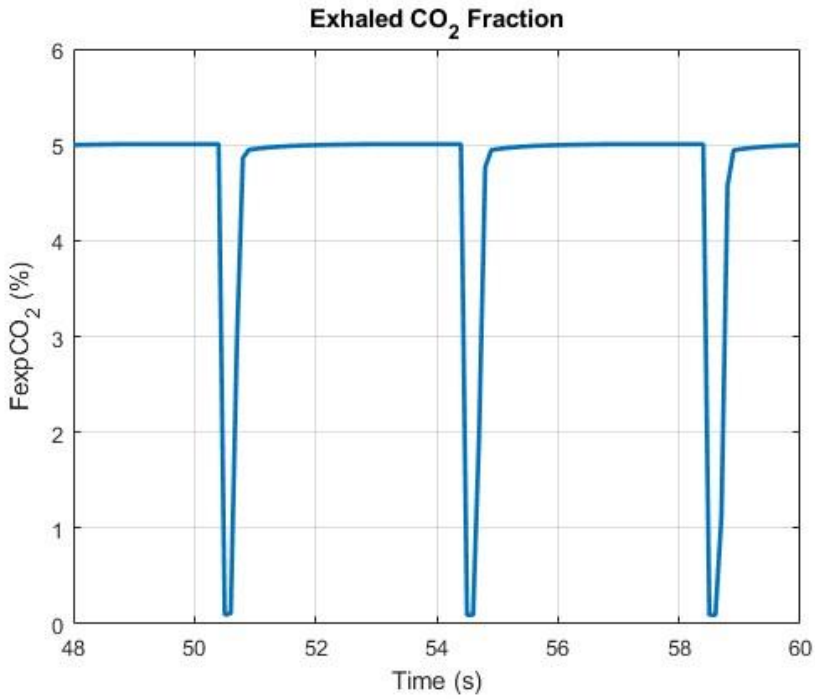

Figure 13: End-tidal CO_2 fraction at CPAP=4 cmH_2O

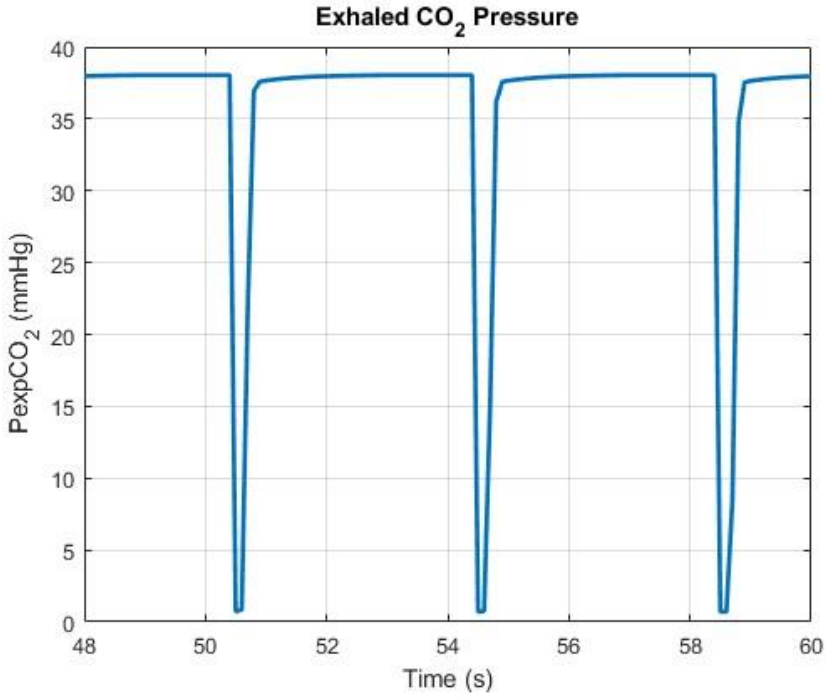

Figure 14: End-tidal CO_2 pressure at CPAP=4 cmH_2O

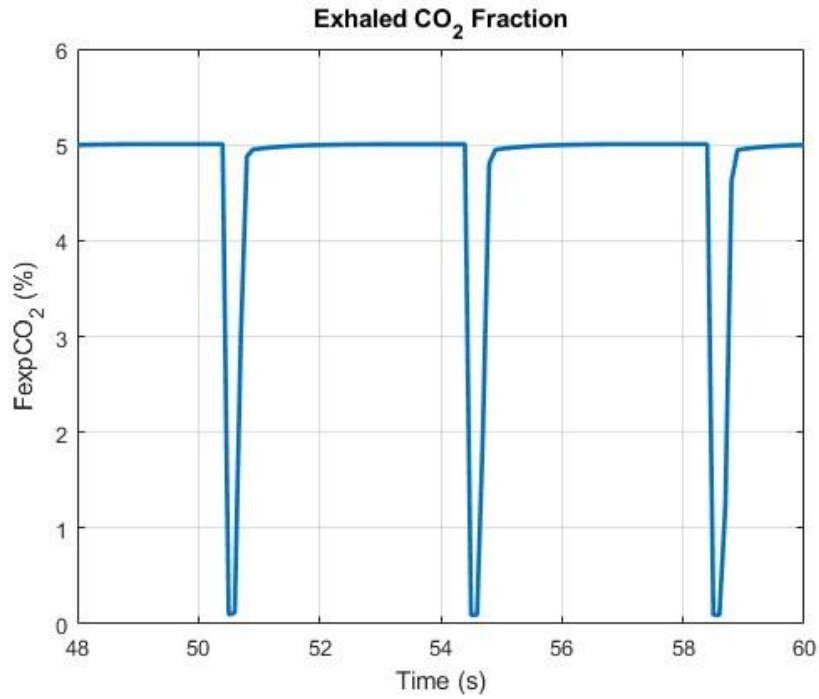

Figure 15: End-tidal CO_2 fraction at CPAP=5 cmH_2O

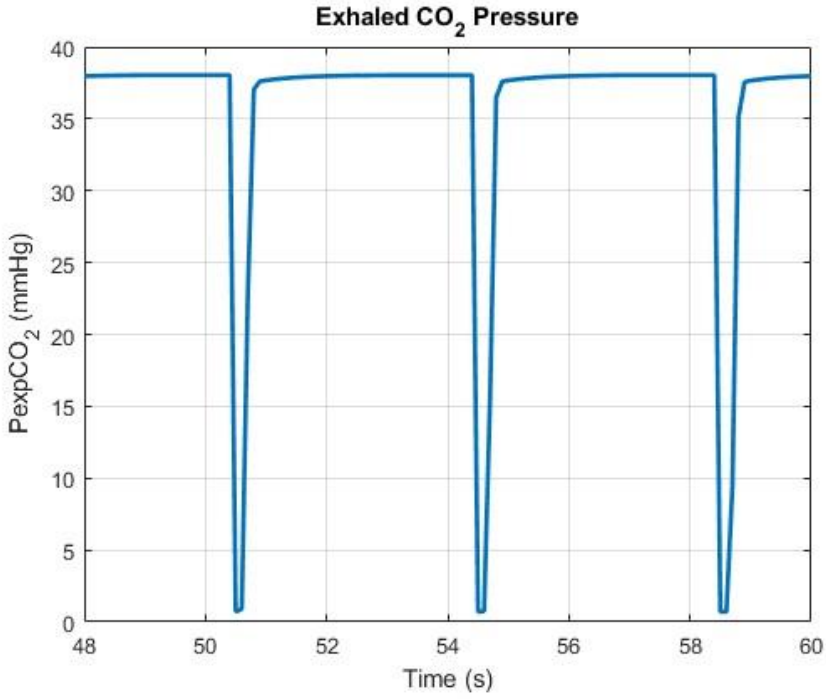

Figure 16: End-tidal CO_2 pressure at CPAP=5 cmH_2O

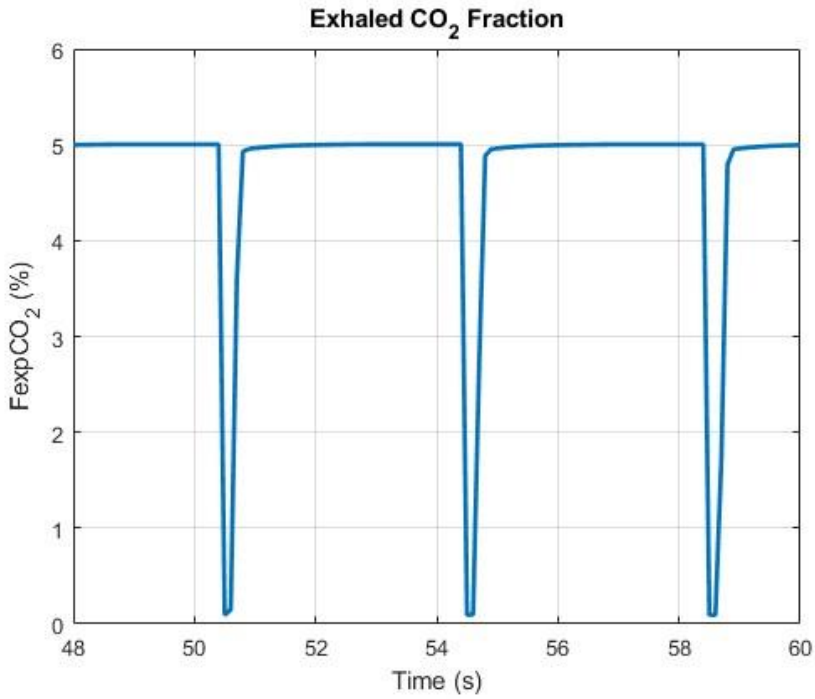

Figure 17: End-tidal CO_2 fraction at CPAP=10 cmH_2O

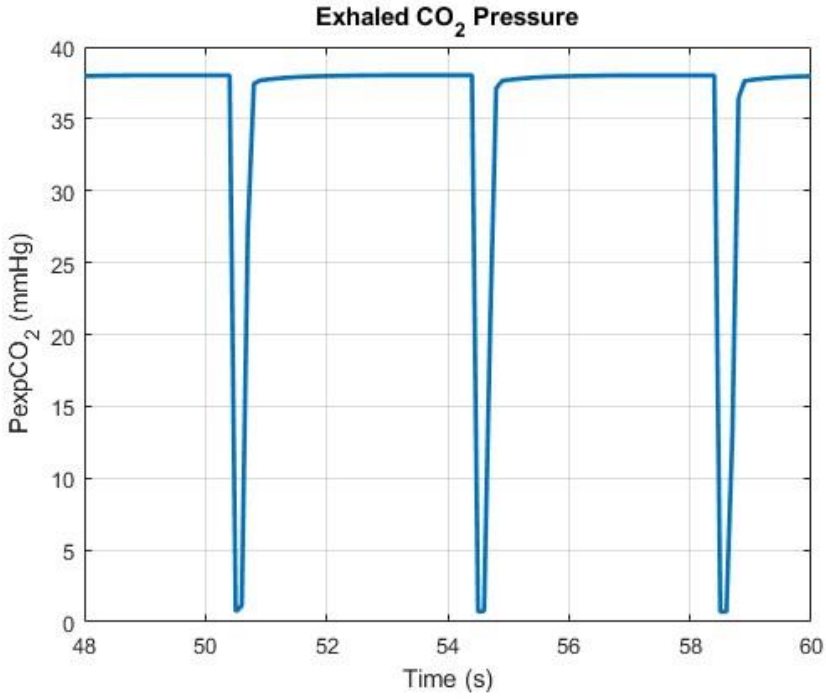

Figure 18: End-tidal CO_2 pressure at CPAP=10 cmH_2O

3.4 Baseline Characteristics

At baseline (spontaneous breathing without CPAP support), the mean end-tidal CO_2 pressure was 35.74 ± 0.73 mmHg, with individual subject values ranging from 35.11 to 36.33 mmHg. This baseline variability reflects the normal physiological range.

3.5 Response to CPAP Application

Upon application of CPAP at 3 cmH_2O, there was an increase in mean end-tidal CO_2 pressure to 37.90 ± 0.48 mmHg, representing an increase of 2.16 mmHg (6.0%) from baseline. This initial rise likely reflects the immediate effects of positive airway pressure on functional residual capacity and the transition to mask breathing with associated changes in dead space.

CPAP masks must demonstrate adequate CO_2 clearance to prevent rebreathing across the CPAP pressure range of 3 to 10 cmH_2O. The maximum increase in end-tidal CO_2 pressure is 6.44 % which is less than the acceptable limit of 20 %.

3.6 Comparison with Bench Test

According to ISO 17510 standards, CPAP masks must demonstrate adequate CO_2 clearance to prevent rebreathing. The benchmark reference value for end-tidal CO_2 pressure in standardised bench tests is approximately 40 mmHg under normal ventilatory conditions.

Thus the simulated value represents a deviation of approximately 5% from the benchmark value, well within the acceptable tolerance for computational model predictions and consistent with the validated accuracy of the simulator.

Table 2: End-tidal CO_2 pressure (mmHg) measured at end-expiration for six virtual subjects at baseline and CPAP pressures of 3, 4, 5, and 10 cmH_2O.

	End-tidal CO_2 pressure (mmHg)						
CPAP (cmH_2O)	**Subject 1**	**Subject 2**	**Subject 3**	**Subject 4**	**Subject 5**	**Subject 6**	**mean±SD**
Baseline	35.11	35.17	35.81	35.92	36.12	36.33	35.74±0.73
3	37.47	37.86	38.27	37.78	37.97	38.08	37.90±0.48
4	37.75	37.84	38.45	37.90	38.08	38.24	38.04±0.46
5	37.71	37.73	38.46	37.95	38.12	38.29	38.04±0.49
10	37.73	37.83	38.46	37.94	38.04	38.18	38.02±0.44

4- Discussion

4.1 CO_2 Dynamics in Bench Testing

The primary determinants of CO_2 pressure in the respiratory system are tidal volume and CO_2 production rate (directly related to O_2 consumption via the respiratory quotient, RQ). In the bench test conditions replicated in our simulations, several key parameters remain constant across all CPAP pressure levels, leading to the observed stability in exhaled CO_2 pressure.

In the standardised bench test configuration:

Constant Flow Dynamics: The flow rate and therefore tidal volume (VT) are maintained constant across all CPAP pressures, eliminating one source of variability in CO_2 clearance.

Fixed Metabolic Parameters: Both O_2 consumption and respiratory quotient (RQ) are held constant in the test setup, resulting in constant CO_2 production rate.

Adequate Dead Space Washout: The mask volume (222 ml) exceeds anatomical dead space (~150 ml), and the combination of fresh gas flow rate and vent flow rate is sufficient to maintain a relatively constant gas fraction within the mask.

Result: The exhaled CO_2 pressure remains approximately constant across the range of CPAP pressures tested

This finding is physiologically consistent with the controlled conditions of the bench testing, where ventilatory parameters are deliberately standardised to isolate the effects of mask venting characteristics.

4.2 Model Accuracy and Acceptable Tolerance

The simulator is a complex, multi-compartmental model founded on well-established physiological equations and anatomical representations. Given the inherent biological variability in human respiratory physiology and the uncertainties in bench test measurements, a deviation of up to 5% from experimental bench test results is considered acceptable for regulatory purposes. This tolerance aligns with:

- Measurement uncertainties in gas analysers

- Guideline recommendations for computational model validation in medical device testing

The validation studies presented demonstrate that the simulator consistently achieves accuracy within this 5% threshold across diverse patient populations and respiratory support modalities, providing robust evidence for its suitability in regulatory applications.

4.3 Implications for Virtual Device Testing

The successful replication of bench test conditions demonstrates the feasibility of in-silico approaches for CPAP mask evaluation. Key advantages of this computational approach include:

Reduced Resource Requirements: Elimination of physical prototypes and test apparatus during iterative design phases

Enhanced Parametric Exploration: The potential for systematic evaluation of mask geometries, vent configurations, and pressure ranges that would be prohibitively expensive in physical testing

Mechanistic Insight: Direct visualisation of gas exchange, mixing, and flow patterns that are difficult or impossible to measure experimentally

Regulatory Pathway: Potential to supplement or partially replace bench testing in regulatory submissions, pending acceptance by regulatory bodies.

4.4 Clinical Reality: Expected Differences

In real-world clinical applications, the relationship between CPAP pressure and CO_2 dynamics differs from the bench test conditions simulated here:

CPAP-Induced Changes in Lung Mechanics: Increasing CPAP pressure elevates functional residual capacity (FRC), which can alter the pressure–volume relationship of the respiratory system.

Ventilatory Response: Higher CPAP pressures typically reduce tidal volume (VT) unless compensated by increased respiratory effort—an undesirable outcome indicating patient–device mismatch or insufficient therapeutic benefit.

Expected Outcome: In the absence of compensatory increases in respiratory drive, rising CPAP pressures would be expected to increase CO_2 pressure due to reduced alveolar ventilation.

4.5 Clinical Implications

The simulator could be extended to model these dynamic patient responses by incorporating respiratory drive modulation and pressure-dependent changes in respiratory mechanics, enabling the prediction of CO_2 accumulation risk in real-world usage scenarios across different CPAP pressure settings.

5- Reliability and Credibility of the Simulator (ASME V&V 40 Framework)

The computational simulator and associated MATLAB code used in this study were developed and evaluated following the principles of ASME V&V 40-2018, which provides a structured framework for assessing the credibility of computational models in medical device applications. This framework ensures that computational models meet the rigorous standards required for regulatory submissions and clinical decision-making.

5.1 Verification

5.1.1 Code Verification

All governing equations were rigorously unit-tested within MATLAB to ensure numerical accuracy and consistency across iterations. Analytical test cases, including steady-state flow conditions and single-compartment pressure–volume loops, were compared against closed-form solutions.

5.1.2 Solution Verification

Time-step convergence analyses were conducted to confirm that simulation outcomes were independent of numerical resolution.

5.2 Validation

5.2.1 Comparative Validation

As detailed in the validation section above, model outputs have been extensively validated against multiple independent datasets from published HFNC and NIV studies. The simulator demonstrated excellent agreement with patient data across key physiological parameters (PaO_2, $PaCO_2$, ΔPpl, VT), with mean absolute percentage errors consistently below 10% and typically below 5% for gas exchange parameters. These multi-study validations encompassed diverse patient populations including healthy subjects, COVID-19 patients, COPD patients, AHRF patients, and sepsis patients, establishing the model's versatility and accuracy across a wide range of respiratory conditions.

5.2.2 Boundary Condition Validation

Input parameters such as flow rate, airway resistance, and lung compliance were systematically compared against experimental measurements and established clinical norms to ensure physiological realism. Reference values from peer-reviewed literature were used to verify that all model inputs fell within documented physiological ranges for the populations being simulated.

5.3 Applicability

The intended context of use—CO_2 rebreathing during CPAP therapy—falls squarely within the model's validated domain of respiratory mechanics and gas exchange. The underlying mathematical formulations and physiological mechanisms governing airway pressures, gas transport, and alveolar ventilation are consistent with those validated in the HFNC and NIV studies. Furthermore, the CPAP pressure range (3–20 cmH_2O) overlaps with the positive airway pressures applied in the validation studies, supporting direct extrapolation of model credibility to this application. The model's demonstrated accuracy in predicting CO_2 dynamics under various respiratory support conditions provides strong evidence for its regulatory relevance in CPAP mask assessment.

5.4 Summary of V&V 40 Compliance

Overall, the simulator meets the credibility goals defined by the ASME V&V 40 framework for medium to high-risk medical device testing applications. The comprehensive verification activities ensure numerical correctness, the extensive validation against clinical data establishes physiological accuracy, the uncertainty quantification demonstrates robustness, and the applicability assessment confirms relevance to the intended use case. This multi-faceted approach establishes high confidence in the simulator's predictive reliability for regulatory submissions and in-silico device testing.

6- Conclusions and Future Work

6.1 Key Findings

This study demonstrates that computational simulation can accurately replicate the CO_2 rebreathing bench test for CPAP masks. Under standardised bench test conditions, CO_2 pressure remains approximately constant across CPAP pressure levels due to:

1. Constant tidal volume (flow rate maintained)
2. Constant O_2 consumption and respiratory quotient (RQ), yielding constant CO_2 production
3. Adequate fresh gas flow and mask volume (> anatomical dead space) to maintain stable gas fractions

The computational simulator, validated against extensive clinical data from HFNC and NIV studies across diverse patient populations, meets ASME V&V 40 credibility requirements for medium-risk medical device applications. Output variability remained within ±5% across physiological ranges, confirming model robustness and regulatory relevance.

6.2 Divergence from Clinical Conditions

Importantly, bench test conditions differ in certain respects from clinical reality. In actual patient use:

Increased CPAP pressure → Higher functional residual capacity (FRC)

Higher FRC → Lower tidal volume (VT), unless compensated by increased respiratory effort (which would be undesirable)

Lower VT → Reduced alveolar ventilation

Expected Clinical Outcome: CO_2 pressure would be expected to rise at higher CPAP pressures in real patients

This mechanistic understanding highlights the limitations of bench testing and suggests opportunities for computational modelling to bridge the gap between standardised testing and real-world validation in patients.

6.3 Future Work

Several promising directions for extending this work include:

Physiological Realism: Simulate realistic patient responses by incorporating more realistic respiratory flow patterns, respiratory drive modulation, and pressure-dependent changes in tidal volume to predict CO_2 accumulation risk across CPAP pressure ranges

Patient Stratification: Develop virtual cohorts representing OSA patients with varying severities, comorbidities (obesity, COPD overlap), and respiratory mechanics to assess mask performance across diverse clinical populations

Mask Design Optimisation: Utilise the validated model for parametric studies exploring vent hole configurations, mask volumes, and geometries to optimise CO_2 clearance while maintaining therapeutic efficacy

Regulatory Pathway Development: Engage with regulatory bodies (FDA, EMA) to establish acceptance criteria and evidence requirements for in-silico testing as a complement or alternative to traditional bench testing

Extended Validation: Conduct prospective validation studies comparing simulator predictions with measurements from human subject trials wearing CPAP masks under controlled conditions

By extending the computational framework to incorporate dynamic patient responses and conducting targeted experimental validation studies, *in-silico* methods have the potential to transform CPAP mask development, reducing time-to-market, minimising animal and human testing burdens, and ultimately improving device safety and efficacy for patients with obstructive sleep apnoea.

References

[1] J. G. Hardman, N. M. Bedforth, A. B. Ahmed, R. P. Mahajan, and A. R. Aitkenhead, "A physiology simulator: validation of its respiratory components and its ability to predict the patient's response to changes in mechanical ventilation.," *Br J Anaesth*, vol. 81, no. 3, pp. 327–332, 1998.

[2] J. G. Hardman and N. M. Bedforth, "Estimating venous admixture using a physiological simulator," *Br J Anaesth*, vol. 82, no. 3, pp. 346–349, 1999.

[3] J. G. Hardman and A. R. Aitkenhead, "Estimation of alveolar deadspace fraction using arterial and end-tidal CO2: a factor analysis using a physiological simulation," *Anaesth Intensive Care*, vol. 27, no. 5, pp. 452–458, 1999.

[4] J. G. Hardman and A. R. Aitkenhead, "Validation of an original mathematical model of CO2 elimination and dead space ventilation," *Anesth Analg*, vol. 97, no. 6, pp. 1840–1845, 2003.

[5] J. G. Hardman and J. S. Wills, "The development of hypoxaemia during apnoea in children: a computational modelling investigation," *BJA: British Journal of Anaesthesia*, vol. 97, no. 4, pp. 564–570, 2006.

[6] A. Das, Z. Gao, P. P. Menon, J. G. Hardman, and D. G. Bates, "A systems engineering approach to validation of a pulmonary physiology simulator for clinical applications.," *J R Soc Interface*, vol. 8, no. 54, pp. 44–55, Jan. 2011, doi:http://dx.doi.org/10.1098/rsif.2010.0224.

[7] J. G. Hardman and H. M. Al-Otaibi, "Prediction of arterial oxygen tension: validation of a novel formula," *Am J Respir Crit Care Med*, vol. 182, no. 3, pp. 435–436, 2010.

[8] S. Saffaran, A. Das, J. G. Laffey, J. G. Hardman, N. Yehya, and D. G. Bates, "Utility of Driving Pressure and Mechanical Power to Guide Protective Ventilator Settings in Two Cohorts of Adult and Pediatric Patients With Acute Respiratory Distress Syndrome: A Computational Investigation.," *Crit Care Med*, vol. 48, no. 7, pp. 1001–1008, Jul. 2020, doi:http://dx.doi.org/10.1097/CCM.0000000000004372.

[9] L. Weaver *et al.*, "High risk of patient self-inflicted lung injury in COVID-19 with frequently encountered spontaneous breathing patterns: a computational modelling

study," *Ann Intensive Care*, vol. 11, no. 1, pp. 1–8, 2021, doi:http://dx.doi.org/10.1186/s13613-021-00904-7.

[10] L. Weaver *et al.*, "Optimising respiratory support for early COVID-19 pneumonia: a computational modelling study," *Br J Anaesth*, vol. 128, no. 6, pp. 1052–1058, 2022.

[11] M. Laviola, A. Das, M. Chikhani, D. G. Bates, and J. G. Hardman, "Computer simulation clarifies mechanisms of carbon dioxide clearance during apnoea," *Br J Anaesth*, vol. 122, no. 3, pp. 395–401, 2019, doi:http://dx.doi.org/https://doi.org/10.1016/j.bja.2018.11.012.

[12] C. Daudre-Vignier, D. G. Bates, T. E. Scott, J. G. Hardman, and M. Laviola, "Evaluating current guidelines for cardiopulmonary resuscitation using an integrated computational model of the cardiopulmonary system," *Resuscitation*, vol. 186, no. January, p. 109758, 2023, doi:http://dx.doi.org/10.1016/j.resuscitation.2023.109758.

[13] D. M. Hannon *et al.*, "Modeling Mechanical Ventilation In Silico-Potential and Pitfalls.," *Semin Respir Crit Care Med*, vol. 43, no. 3, pp. 335–345, Jun. 2022, doi:http://dx.doi.org/10.1055/s-0042-1744446.

[14] A. Das *et al.*, "In Silico Modeling of Coronavirus Disease 2019 Acute Respiratory Distress Syndrome: Pathophysiologic Insights and Potential Management Implications," *Crit Care Explor*, vol. 2, no. 9, p. e0202, 2020, doi:http://dx.doi.org/10.1097/cce.0000000000000202.

[15] S. Saffaran *et al.*, "Inhaled sGC modulator can lower pH in patients with COPD without deteriorating oxygenation," *CPT Pharmacometrics Syst Pharmacol*, vol. 7, no. 8, pp. 491–498, 2018.

[16] M. Chikhani, A. Das, M. Haque, W. Wang, D. G. Bates, and J. G. Hardman, "High PEEP in acute respiratory distress syndrome: quantitative evaluation between improved arterial oxygenation and decreased oxygen delivery.," *Br J Anaesth*, vol. 117, no. 5, pp. 650–658, Nov. 2016, doi:http://dx.doi.org/10.1093/bja/aew314.

[17] L. Weaver *et al.*, "Digital Twins of Acute Hypoxemic Respiratory Failure Patients Suggest a Mechanistic Basis for Success and Failure of Noninvasive Ventilation," *Crit Care Med*, May 2024, doi:http://dx.doi.org/10.1097/CCM.0000000000006337.

[18] H. Shamohammadi *et al.*, “Airway pressures generated by high flow nasal cannula in patients with acute hypoxemic respiratory failure: a computational study,” *Respir Res*, vol. 26, no. 1, p. 9, 2025, doi:http://dx.doi.org/10.1186/s12931-025-03096-x.

[19] H. Shamohammadi *et al.*, “Digital twins suggest a mechanistic basis for differing responses to increased flow rates during high-flow nasal cannula therapy.,” *Intensive Care Med Exp*, vol. 13, no. 1, p. 66, Jun. 2025, doi:http://dx.doi.org/10.1186/s40635-025-00773-5.

[20] B. Lachmann, “Open up the lung and keep the lung open,” *Intensive Care Med*, vol. 18, no. 6, pp. 319–321, Jun. 1992, doi:http://dx.doi.org/10.1007/BF01694358.

[21] K. G. Hickling, “The pressure-volume curve is greatly modified by recruitment. A mathematical model of ARDS lungs,” *Am J Respir Crit Care Med*, vol. 158, no. 1, pp. 194–202, 1998, doi:http://dx.doi.org/10.1164/AJRCCM.158.1.9708049.

[22] J. H. T. Bates and C. G. Irvin, “Time dependence of recruitment and derecruitment in the lung: a theoretical model,” *J Appl Physiol (1985)*, vol. 93, no. 2, pp. 705–713, 2002, doi:http://dx.doi.org/10.1152/JAPPLPHYSIOL.01274.2001.

[23] B. E. Marshall, W. R. Clarke, A. T. Costarino, L. Chen, F. Miller, and C. Marshall, “The dose-response relationship for hypoxic pulmonary vasoconstriction,” *Respir Physiol*, vol. 96, no. 2–3, pp. 231–247, May 1994, doi:http://dx.doi.org/10.1016/0034-5687(94)90129-5.

[24] J. W. Severinghaus, “Simple, accurate equations for human blood O2 dissociation computations,” *J Appl Physiol Respir Environ Exerc Physiol*, vol. 46, no. 3, pp. 599–602, 1979, doi:http://dx.doi.org/10.1152/JAPPL.1979.46.3.599.

[25] J. W. Severinghaus, “Blood gas calculator,” *J Appl Physiol*, vol. 21, no. 3, pp. 1108–1116, 1966, doi:http://dx.doi.org/10.1152/JAPPL.1966.21.3.1108.

[26] A. R. Douglas, N. L. Jones, and J. W. Reed, “Calculation of whole blood CO2 content,” *https://doi.org/10.1152/jappl.1988.65.1.473*, vol. 65, no. 1, pp. 473–477, 1988, doi:http://dx.doi.org/10.1152/JAPPL.1988.65.1.473.

[27] G. J. McHardy, “The relationship between the differences in pressure and content of carbon dioxide in arterial and venous blood.,” *Clin Sci*, vol. 32, no. 2, pp. 299–309, Apr. 1967.

[28] G. R. Kelman and J. F. Nunn, “Nomograms for correction of blood Po2, Pco2, pH, and base excess for time and temperature.,” *J Appl Physiol*, vol. 21, no. 5, pp. 1484–1490, Sep. 1966, doi:http://dx.doi.org/10.1152/jappl.1966.21.5.1484.

[29] O. Siggaard-Andersen, “The van Slyke equation.,” *Scand J Clin Lab Invest Suppl*, vol. 146, pp. 15–20, 1977, doi:http://dx.doi.org/10.3109/00365517709098927.

[30] J. S. Mecklenburgh and W. W. Mapleson, “Ventilatory assistance and respiratory muscle activity. 2: Simulation with an adaptive active (‘aa’ or ‘a-squared’) model lung,” *Br J Anaesth*, vol. 80, no. 4, pp. 434–439, 1998, doi:http://dx.doi.org/10.1093/BJA/80.4.434.

[31] A. Albanese, L. Cheng, M. Ursino, and N. W. Chbat, “An integrated mathematical model of the human cardiopulmonary system: model development,” *American Journal of Physiology-Heart and Circulatory Physiology*, vol. 310, no. 7, pp. H899–H921, Apr. 2016, doi:http://dx.doi.org/10.1152/ajpheart.00230.2014.

[32] H. Shamohammadi *et al.*, “Airway pressures generated by high flow nasal cannula in patients with acute hypoxemic respiratory failure: A computational study,” 2024.

[33] R. Tonelli *et al.*, “Early Inspiratory Effort Assessment by Esophageal Manometry Predicts Noninvasive Ventilation Outcome in De Novo Respiratory Failure: A Pilot Study,” *Am J Respir Crit Care Med*, vol. 202, no. 4, pp. 558–567, 2020, doi:http://dx.doi.org/10.1164/rccm.201912-2512OC.

[34] R. Tonelli *et al.*, “Inspiratory Effort and Lung Mechanics in Spontaneously Breathing Patients with Acute Respiratory Failure due to COVID-19: A Matched Control Study.,” *American journal of respiratory and critical care medicine*, vol. 204, no. 6. United States, pp. 725–728, Sep. 2021. doi:http://dx.doi.org/10.1164/rccm.202104-1029LE.

[35] T. Mauri *et al.*, “Optimum support by high-flow nasal cannula in acute hypoxemic respiratory failure: effects of increasing flow rates,” *Intensive Care Med*, vol. 43, no. 10, pp. 1453–1463, 2017, doi:http://dx.doi.org/10.1007/s00134-017-4890-1.

[36] D. Slobod *et al.*, “Effects of an asymmetrical high flow nasal cannula interface in hypoxemic patients.,” *Crit Care*, vol. 27, no. 1, p. 145, Apr. 2023, doi:http://dx.doi.org/10.1186/s13054-023-04441-6.

[37] T. Mauri *et al.*, “Respiratory Drive in Patients with Sepsis and Septic Shock: Modulation by High-flow Nasal Cannula.,” *Anesthesiology*, vol. 135, no. 6, pp. 1066–1075, Dec. 2021, doi:http://dx.doi.org/10.1097/ALN.0000000000004010.

[38] R. L. Parke, A. Bloch, and S. P. McGuinness, “Effect of very-high-flow nasal therapy on airway pressure and end-expiratory lung impedance in healthy volunteers,” *Respir Care*, vol. 60, no. 10, pp. 1397–1403, 2015, doi:http://dx.doi.org/10.4187/respcare.04028.